EXPERIMENTAL STUDY ON THE MECHANISM OF FAVOURABLE INTERFERENCES OF BODY STRAKES

Xia Xuejian, Liu Xiaofeng, Feng Yanan

Fluid Mechanics Institute,
Beijing University of Aeronautics and Astronautics
Beijing, China, 100083

Abstract

Wind tunnel flow field measurements and water channel flow visualizations were conducted to study the phenomena and the mechanism of favourable interferences among body strake vortex, wing leading-edge vortex and body vortex, such as to induce, to move around, and to merge each other. The essential result of the favourable interferences is to delay the wing leading-edge vortex bursting. In the present experiment the space flow field was measured in detail by using the seven-hole probe in wind tunnel. From quantitative investigations and analyses, the main mechanism of achieving favourable interferences is presented.

I. Introduction

A modern fighter aircraft is being expected to improve the maneuverability at high angles of attack. It is beneficial to increase C_{Lmax} and the stall angle of attack to achieve the above aim. As we know, for the slender wing with sharp leading-edge and large sweep angle, the contribution of leading-edge vortex plays an important role in the total lift. So it is interested to find some methods to delay the wing vortex bursting in order to reduce the loss of lift caused by vortex bursting. Our previous study shows that as a pair of body strakes with small area mounted in the front of the leading-edge of the wing, the wing leading-edge vortex bursting can be effectively delayed due to the favourable interferences among body strake vortex, wing vortex and body vortex. And the lift coefficient at high angles of attack as well as the stall angle can be increased correspondingly. Then the aerodynamic characteristics can be improved at high angles of attack [1-4]. Until recently, there are not many papers on the mechanism of favourable interferences among vortices. In the present experiment, the vortex flow fields for model with and without body strakes were measured in detail by using seven-hole probe. Analyses of flow field measured in different sections were conducted in order to quantitatively understand the mechanism of favourable interferences among vortices.

II. Apparatus, Models and Test Techniques

Measurements of vortex flow field were carried out in the low-speed wind tunnel of BUAA, which has an open elliptical test section with 1.02m major axis and 0.76m minor axis, at a Reynolds number of 1.44×10^6(1/m).

The measurements of pressure and velocity field were performed at the angle of attack of 24° by using seven-hole probe which is demonstrated to have the capability to determine flow angles up to 80 degrees relative to its axis[5,6]. The probe was fixed at a five dimensional displacement mechanism which is controlled by using grating technology. The pressure signals were acquired and processed by a system consisted of PDRC strain transducer, Preston MX-B channel amplifier, A/D(D/A) converter and a PC microcomputer.

The cross-sections in which measurements were conducted are perpendicular to the longitudinal axis of the configuration body. The step between measured points in the sections is taken 5mm in the area far away from the vortex core, 2mm in the area near the vortex core and 1mm in or in close vicinity of the vortex core.

In the present paper, velocity vector is given in three dimensionless components fixed in the body axes system, i.e., $\bar{u}_b$, $\bar{v}_b$, $\bar{w}_b$. Local total pressure coefficient C_{pol} and static pressure coefficient C_{psl} are defined as:

$$C_{pol} = (p_{ol}-p_\infty)/q_\infty \ ,$$

$$C_{psl} = (p_{sl}-p_\infty)/q_\infty \ ,$$

where p_∞ and q_∞ are the static and dynamic pressure at upstream infinity respectively.

The configurations tested are sketched in Fig.1. The Basic Configuration is a blended wing-body configuration with elliptical cross-sectional body, double tail and double-delta wing. Body strake 1# is mounted in the same plane of the wing and there is a short distance between the strake trailing-edge and the wing leading-edge. Body strake 2# is mounted in the plane slightly above the wing and its trailing-edge is very close to the wing leading-edge in the longitudinal direction. Configurations with body strake 1# and 2# hereafter are denoted as "Configuration 1#" and "Configuration 2#" respectively.

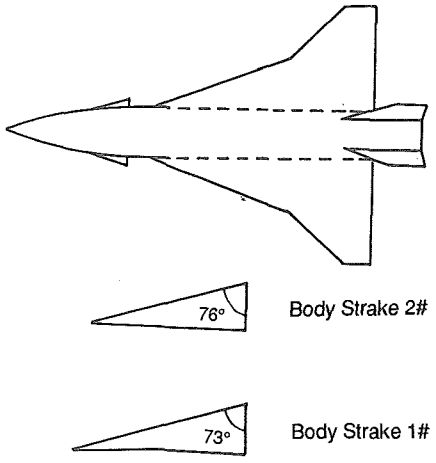

Fig.1 Configurations and Body Strakes Tested

Flow visualization experiments were carried out at a Reynolds number of about 8.3×10^4(1/m) in the water channel of BUAA, which has a test section of $0.4\times0.4m^2$ and free stream velocity of 0.1m/s. The visualization of vortex flow pattern was performed by means of dyeing technique to observe the interferential phenomena among body strake vortex, wing leading-edge vortex and body vortex, particularly to observe the effects of body strakes on wing leading-edge vortex bursting.

III. Results of Vortex Flow Field Measurements

Total Pressure Distributions (C_{pol})

1. Basic Configuration

Fig.2 shows the total pressure distributions at sections of

$\bar{x}$=0.25 and 0.50 of the Basic Configuration. The wing vortex and the body vortex can be seen clearly in the plots. A secondary separated flow near the wing leading-edge can also be found in Fig.2(b). The comparison of C_{pol} spanwise distribution through the wing vortex core center at different sections of the Basic Configuration is shown in Fig.3. It can be seen that at sections of $\bar{x}$ =0.25 and 0.45 the total pressure varied rapidly. The vortex core do exist. But at sections of $\bar{x}$=0.50 and 0.55, the size of the wing vortex core, which is listed in Table 2, increases apparently. It seems that at sections of $\bar{x}$=0.50 to 0.55, the wing vortex bursting may occur. The total pressure coefficient at the wing vortex center changes greatly from -8.28 at section of $\bar{x}$=0.25 to -5.55 at section of $\bar{x}$=0.50. It follows that the features of vortex bursting is evident in section of $\bar{x}$=0.50 for the Basic Configuration. This is consistent with the result of flow visualization in the water channel.

2. Configuration 1#

Distributions of C_{pol} at sections of $\bar{x}$= 0.25, 0.50 and 0.70 of Configuration 1# are plotted in Fig.4. At these sections only two vortices can be distinguished. One is the wing leading-edge vortex, the other is the vortex which is merged by the body vortex and the strake vortex (hereafter denoted as body-strake vortex). Fig.5 shows the total pressure spanwise distribution through the wing vortex center at sections of $\bar{x}$= 0.25, 0.50, 0.65, 0.70 and 0.80 of Configuration 1#. It is observed that at section of $\bar{x}$ =0.50 the vortex core is still intensive. But at section of $\bar{x}$=0.70 the size of the vortex core expands obviously. More expansion occurs at section of $\bar{x}$ =0.80. And these two curves are both in the shape of sawtooth. It seems that at section of $\bar{x}$=0.65, the state of wing vortex begins to approach the condition of vortex bursting which was described by Leibovich[7]. This phenomenon shows no difference with the tendency obtained in water channel experiment.

3. Configuration 2#

Distribution and comparison of C_{pol} of Configuration 2# are shown in Fig.6 and 7 respectively. At section of $\bar{x}$=0.50 , the wing vortex did not burst for Configuration 2#.

To summarize the general characteristics of vortex development for the three configurations, it is found that the body vortex, strake vortex or body-strake vortex move around the wing vortex. The size of vortex core gradually increases before vortex bursting. Once the vortex bursts, the vortex core expands obviously and the total pressure at the vortex center recovers. Earnshaw[8] pointed out that before vortex bursting, $(d/s)(\bar{x})^{1/2}$ remains a constant, where d is a diameter of the vortex core, s is a length of the half span of the wing, $\bar{x}$ is a dimensionless length of the wing root chord. For a same configuration, the values of $(d/s)(\bar{x})^{1/2}$ at different sections are almost identical before vortex bursting, see Table 2. The result of the present experiments confirmed the viewpoint presented by Earnshaw.

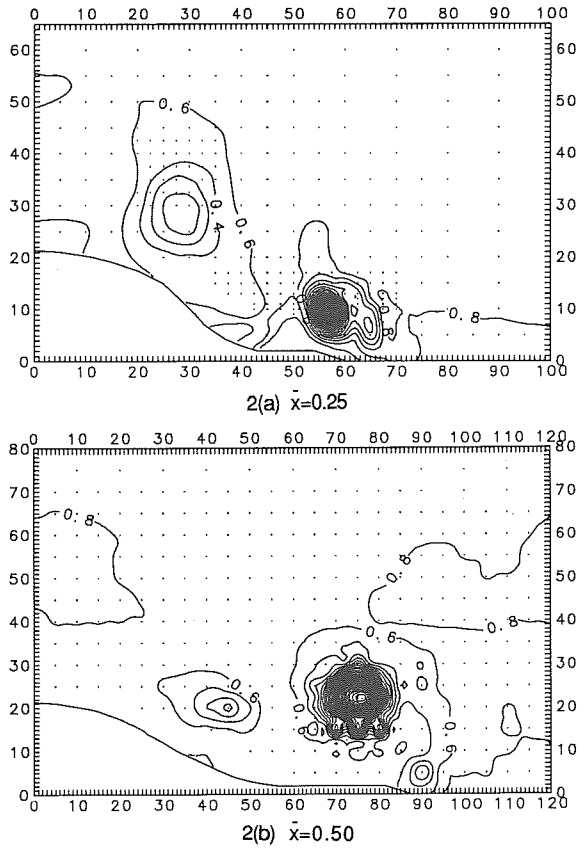

Fig.2 Distributions of Total Pressure C_{pol} at Different Sections of the Basic Configuration

Static Pressure Distributions (C_{psl})

For the Basic Configuration, static pressure distribution and comparison are shown in Fig.8 and 9. It can be seen that static

Table 1. Total Pressure C_{pol}, Static Pressure C_{psl} And Axial Velocity $\bar{u}_b$ Extreme Values And Their Corresponding Coordinates (α=24°)

Model	Test Section $\bar{x}$	Min. C_{pol} & (y,z)	Min. C_{psl} & (y,z)	Max.(Min.) $\bar{u}_b$ & (y,z)
Basic Configuration	0.25	-8.28(10,57)	-8.29(10,57)	-0.01(10,57)
	0.45	-6.12(20,73)	-6.47(20,73)	-0.19(20,72)
	0.50	-5.55(22,76)	-5.78(22,76)	-0.01(22,75)
	0.55	-3.94(25,80)	-4.03(25,80)	-0.07(25,80)
Configuration 1#	0.25	-6.53(10,59)	-9.69(10,61)	2.05(9,59)
	0.50	-4.70(21,75)	-12.00(20,76)	2.73(20,76)
	0.65	-4.70(30,86)	-6.16(29,87)	0.70(30,85)
	0.70	-4.29(33,89)	-4.38(33,89)	-0.16(33,89)
	0.80	-2.22(40,100)	-2.30(39,99)	-0.17(40.99)
Configuration 2#	0.25	-4.60(11,59)	-8.63(11,59)	2.21(12,59)
	0.50	-4.31(25,74)	-9.59(25,74)	2.37(25,73)

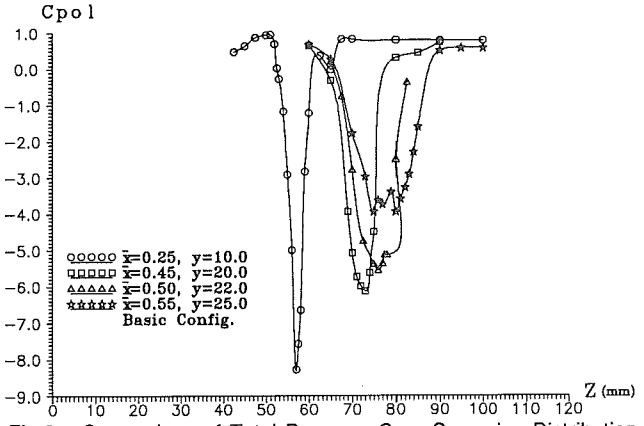

Fig.3 Comparison of Total Pressure Cp_{pl} Spanwise Distribution through the Wing Vortex Center at Different Sections of the Basic Configuration

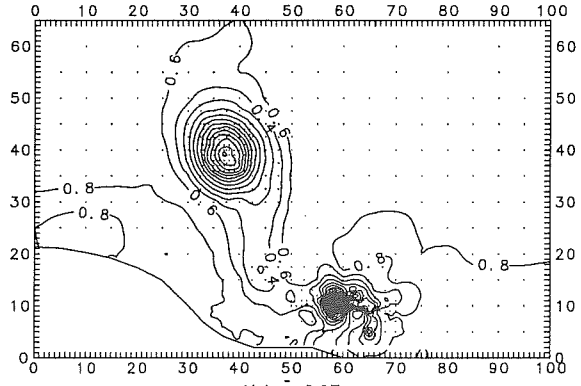

4(a) $\bar{x}$=0.25

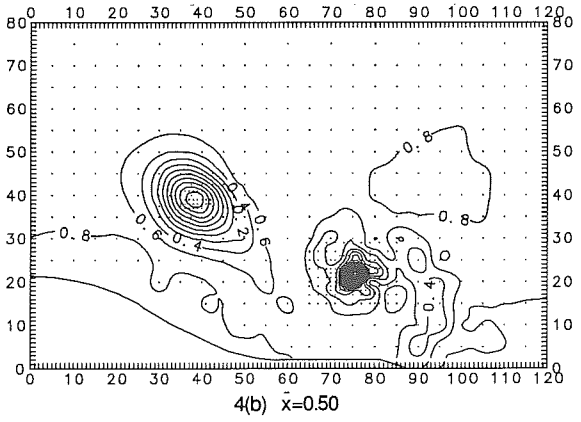

4(b) $\bar{x}$=0.50

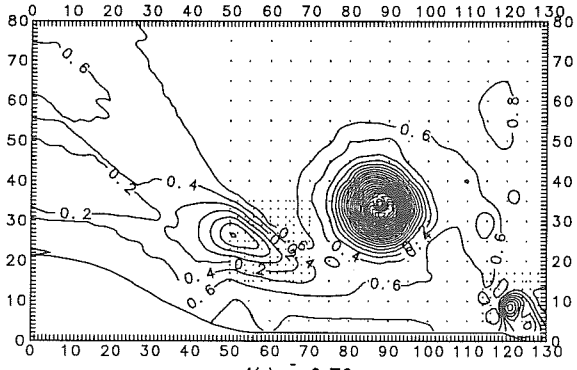

4(c) $\bar{x}$=0.70

Fig.4 Distributions of Total Pressure Cp_{pl} at Different Sections of Configuration 1#

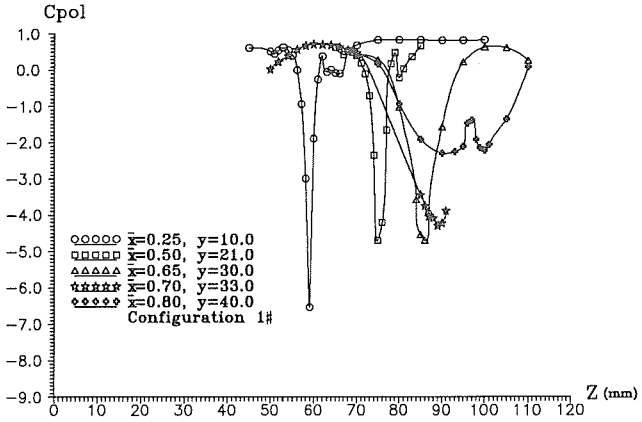

Fig.5 Comparison of Total Pressure Cpol Spanwise Distribution through the Wing Vortex Center at Different Sections of Configuration 1#

pressure coefficient at the wing vortex center increases along the chordwise direction. The static pressure in the vortex core recovers rapidly as vortex bursting occurs. Therefore, the contour lines of static pressure look rarefied at section of $\bar{x}$=0.50.

Fig.10 plots the distribution of static pressure at sections of $\bar{x}$=0.25, 0.50 and 0.70 of Configuration 1#. Comparing with the Basic Configuration, the contour lines of static pressure of Configuration 1# at the wing vortex core still remain intensive at section of $\bar{x}$ =0.50. Then, the contour lines become rarefied at section of $\bar{x}$=0.70. Spanwise distribution of static pressure through the wing vortex center of Configuration 1# is shown in

Table 2. Wing Vortex Location and Its Core Diameter (α=24°)

Model	Test Section $\bar{x}$	Wing Vortex Core Diameter d (mm)	$(d/s)(\bar{x})^{1/2}$	Wing Vortex Coordinates (y,z)	Strake(Body) Vortex Coordinates (y,z)
Basic Configuration	0.25	6.5	0.12	(10,57)	(28,29)
	0.50	15.5	0.20	(22,76)	(20,45)
Configuration 1#	0.25	5	0.09	(10,59)	(40,37.5)
	0.50	6	0.08	(21,75)	(38,39)
	0.70	22	0.20	(33,89)	(27,50)
Configuration 2#	0.25	5.5	0.10	(11,59)	(31,37)
	0.50	6.5	0.09	(25,74)	(20,50)

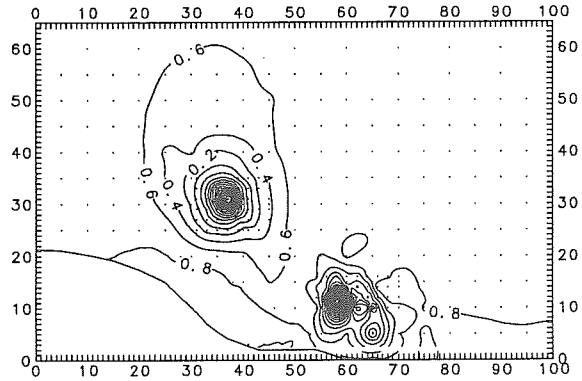

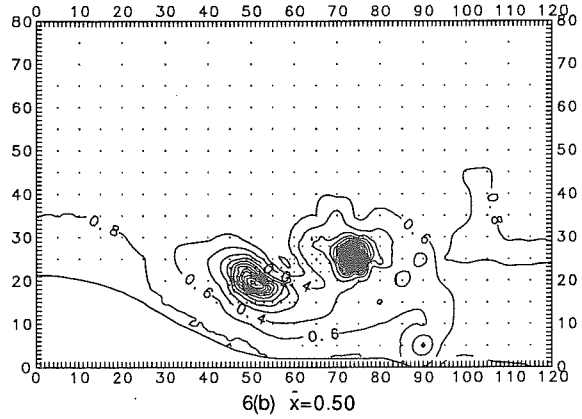

Fig.6 Distributions of Total Pressure Cp_{0l} at Different Sections of Configuration $2^{\#}$

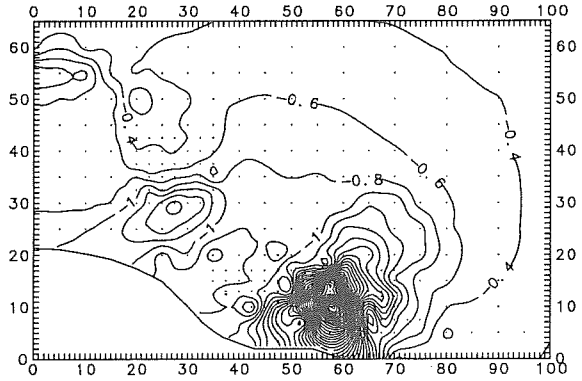

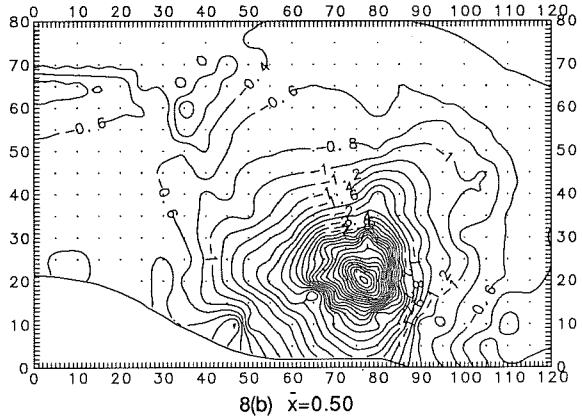

Fig.8 Distributions of Static Pressure Cp_{sl} at Different Sections of the Basic Configuration

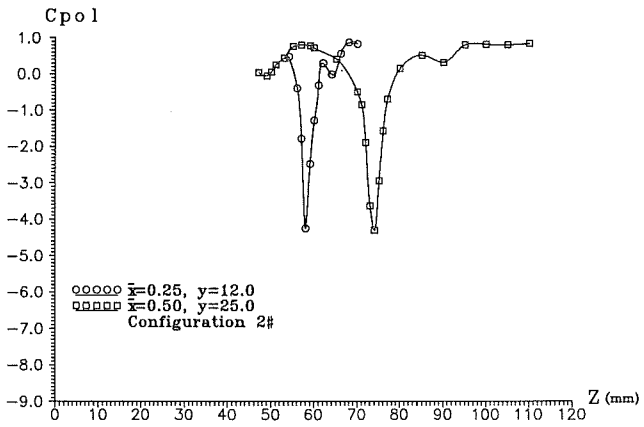

Fig.7 Comparison of Total Pressure Cp_{0l} Spanwise Distribution through the Wing Vortex Center at Different Sections of Configuration $2^{\#}$

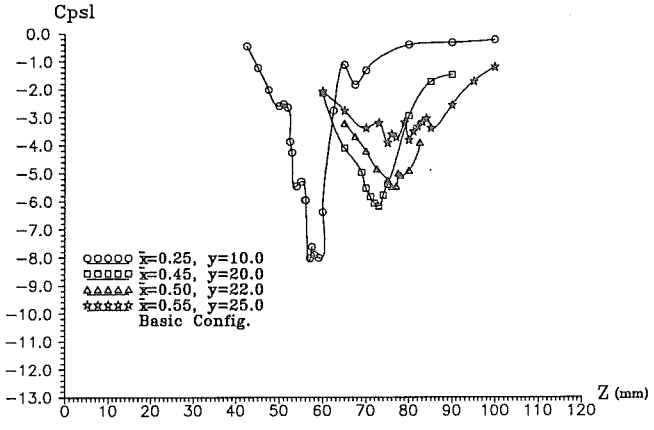

Fig.9 Comparison of Static Pressure Cp_{sl} Spanwise Distribution through the Wing Vortex Center at Different Sections of the Basic Configuration

Fig.11. It is found that before the wing vortex bursting the static pressure at the vortex center of Configuration $1^{\#}$ reduced greatly from section of $\bar{x}$=0.25 to section of $\bar{x}$=0.50 along chordwise direction. When the wing vortex approaches bursting (at section of $\bar{x}$ =0.65), the static pressure recovers. After the bursting occurs (at sections of $\bar{x}$=0.70 and 0.80), the static pressure further recovers, and the curve of static pressure goes up and down near the wing vortex center.

For Configuration $2^{\#}$, the characteristic of the static pressure is similar to that of Configuration $1^{\#}$.

Velocity Distributions

Velocity vector distributions of the Basic Configuration, Configuration $1^{\#}$ and Configuration $2^{\#}$ are given in Fig.12, 13 and 14. In the velocity vector diagrams, except the case of the Basic Configuration at section of $\bar{x}$=0.50, the wing vortex exhibits high rotational speed, which is a typical characteristic of vortex flow. But for the Basic Configuration at section of $\bar{x}$=0.50, the characteristic of velocity vector in the range of wing vortex is quite different from other cases and shows the feature of vortex bursting.

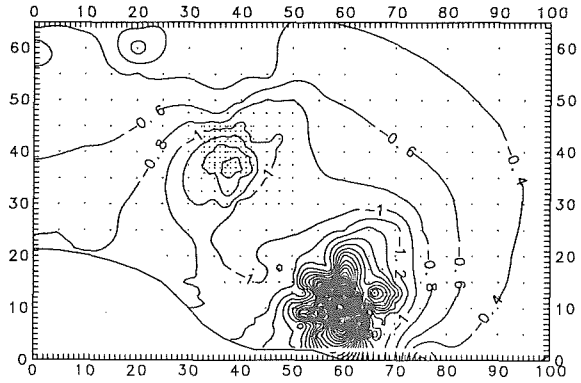

10(a) $\bar{x}$=0.25

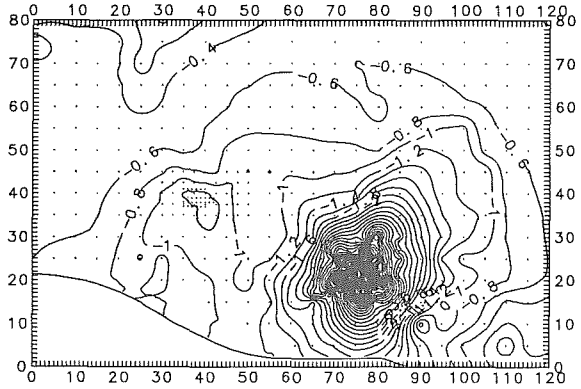

10(b) $\bar{x}$=0.50

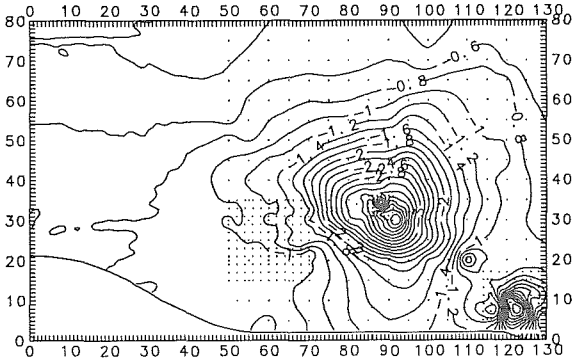

10(c) $\bar{x}$=0.70

Fig.10 Distributions of Static Pressure Cp_{sl} at Different Sections of Configuration 1#

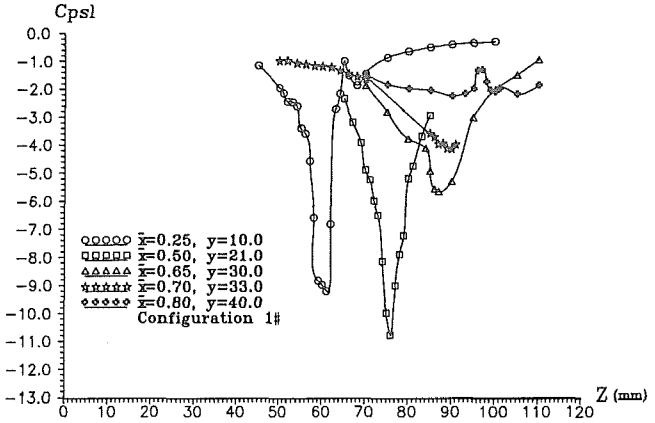

Fig.11 Comparison of Static Pressure Cp_{sl} Spanwise Distribution through the Wing Vortex Center at Different Sections of Configuration 1#

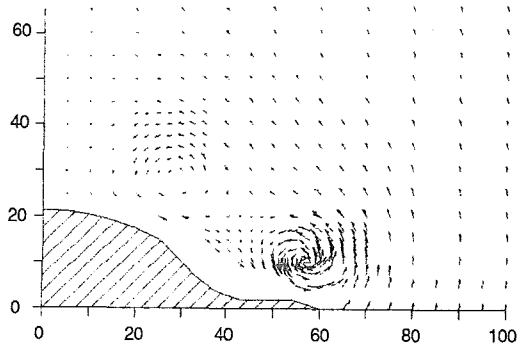

12(a) $\bar{x}$=0.25

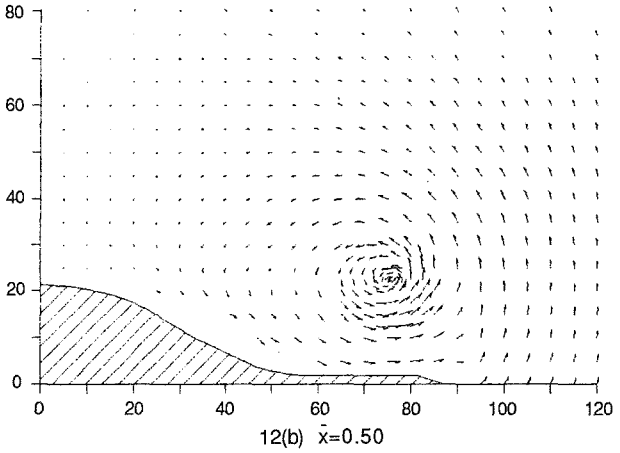

12(b) $\bar{x}$=0.50

Fig.12 Velocity Vector Distributions at Different Sections of the Basic Configuration

In the present experiments the vortex flow fields of all the three configurations manifest general characters of vortex flow. The interferential phenomena of vortices include inducing, moving around and merging each other. Before vortex bursting, the total pressure gradient in vortex core is quite high. The curve of total pressure distribution along vortex radius is steep and smooth. The axial velocity profile shows the form of jet flow in the vortex core. Once the wing vortex bursts, the total pressure will increase , and the curve of total pressure distribution becomes turbulent in the vortex core. Meanwhile, the axial velocity decreases rapidly, even approaches zero, or in the utmost cases, adverse flow occurs in the vortex center. In other words, the axial velocity distribution appears in wake flow profile when the vortex bursts (see Fig.15(c)).

IV. The Mechanism of Effect of Body Strake

The flow field around the Basic Configuration is quite complicated because of the interference between wing vortex and body vortex. The interaction among vortices is more complicated due to the presence of strake vortex as strake is added. As a result, however, the presence of strake vortex effectively improve the aerodynamic characteristics at high angles of attack[2-4].

For the wing with large sweep angle and sharp leading-edge, the leading-edge vortex bursting is an unfavourable factor to

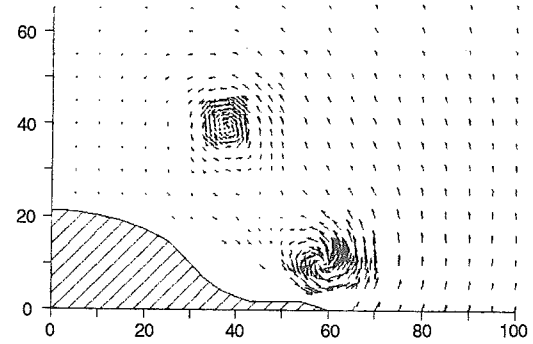

13(a) $\bar{x}$=0.25

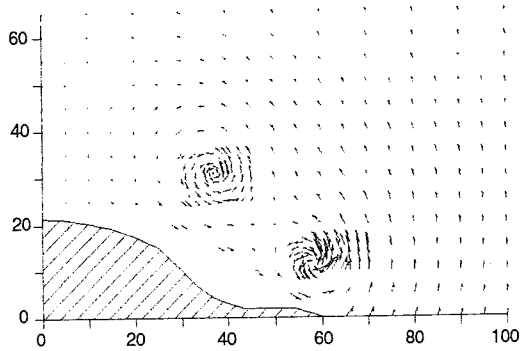

14(a) $\bar{x}$=0.25

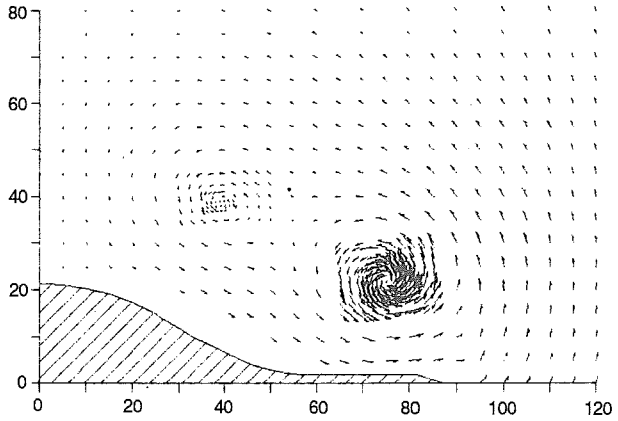

13(b) $\bar{x}$=0.50

Fig.13 Velocity Vector Distributions at Different Sections of Configuration 1#

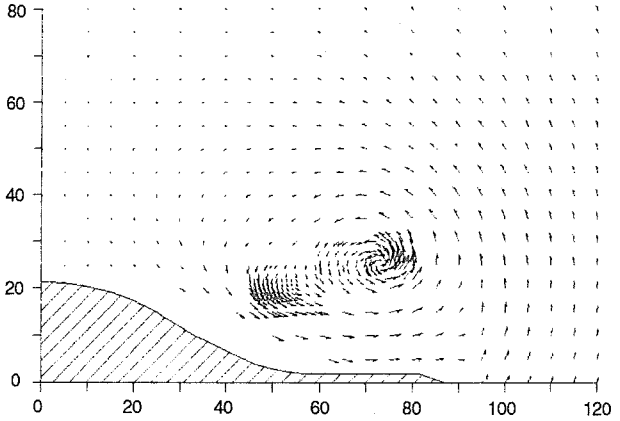

14(b) $\bar{x}$=0.50

Fig.14 Velocity Vector Distributions at Different Sections of Configuration 2#

aerodynamic characteristics at high angles of attack. From our previous experimental results, it has been found that the body strake can delay the wing leading-edge vortex bursting efficiently. This is one of the reasons why the aerodynamic characteristics can be improved at high angles of attack due to the presence of body strake. The mechanism of the body strake to delay the wing vortex bursting is mainly as follows:

1. Flow Fluid in the Vortex Core Gains Additional Energy due to the Effect of Body Strake Vortex.

The comparison of total pressure coefficient for three configurations (see Fig.15(a)) indicates that for Configuration 1# and Configuration 2#, the total pressure in the vortex core increases obviously. If the static pressure did not increases, then the flow fluid in the vortex core must gain more dynamic energy. So flow fluid has more energy to overcome adverse pressure gradient to maintain vortex flow go downstream, and thereby to delay the vortex bursting. In fact, for configurations with body strakes the static pressure decreases while the total pressure increases if compared with the Basic Configuration (see Fig 15(b)). Thus, the flow fluid in the vortex really obtains additional energy. Fig.15(c) shows the axial velocity $\bar{u}_b$ spanwise distribution through the vortex center. It is clear that the body strakes make the axial velocity increase considerably, and the velocity profile changes from the wake flow profile to the jet flow profile due to the presence of body strakes.

2. Body Strakes Enhance the Stability of Wing Vortex.

One of the theories to distinguish the stability of vortex flow, i.e., stagnation criterion presented by Bossel[9] is stated that,

$$tg\varphi=v_\tau/v_b$$

where v_τ and v_b are the tangential and axial velocities of vortex flow at the edge of vortex core, $\varphi=arctg(v_\tau/v_b)$ is a spiral angle. The larger the value of φ is, the more unstable the vortex flow is. If φ>44.8°~54.8°, then the axial velocity in the vortex core will decrease. Finally, stagnation and adverse flow will occur. This means that the vortex bursting occurs. In the present experiments, it is found that for configurations with body strakes the spiral angle φ has been reduced, as shown in Table 3. Then the stability of wing vortex flow is enhanced due to the effect of body strake vortex.

Besides, based on the calculated result by Wedemeyer[10] for the flow field around the delta wing, it is obtained that for delta wing vortex flow is stable as k>1.16 and unstable as k<0.8~1.16, where k is a parameter of velocity profile of leading-edge vortex core. We calculated the value of k for double-delta wing of our configuration by using the following equation,

$$v_\tau/v_b=(k+0.5)^{1/2}\cdot k$$

It is found that at the section of $\bar{x}$=0.50, the value of k increases from 0.98 related to the case of the Basic Configuration, to 3.50 related to the case of Configuration 1#. From this result it can be concluded that the stability of vortex flow for configurations with body strakes is enhanced as the value of k increases.

To enhance the stability of wing vortex will result in the delay of wing vortex bursting, and therefore the wing vortex lift will be increased at high angles of attack.

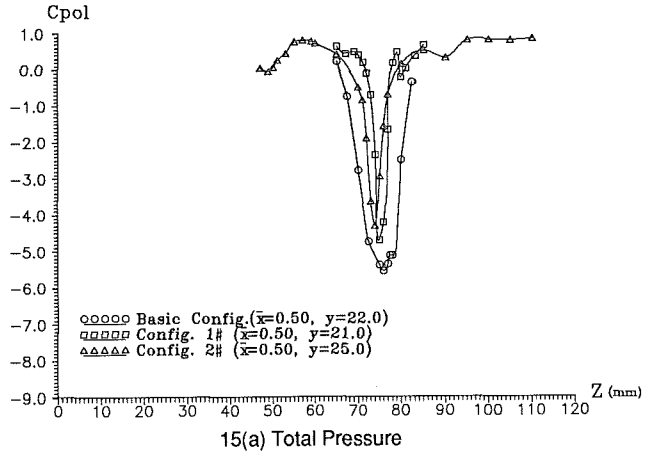

15(a) Total Pressure

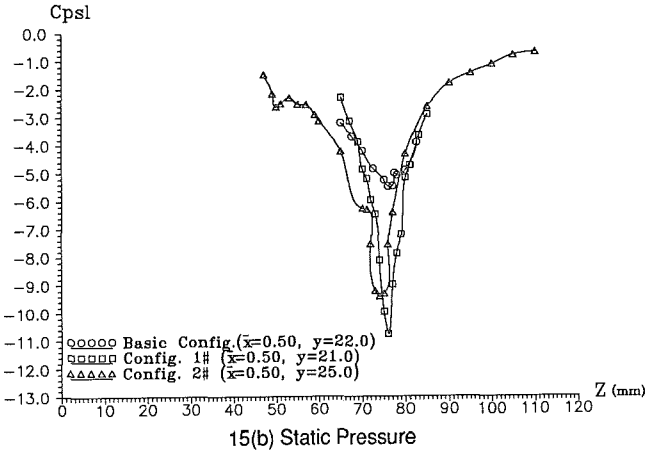

15(b) Static Pressure

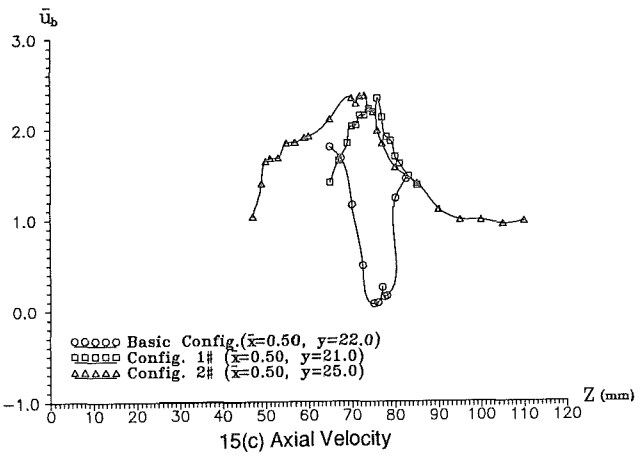

15(c) Axial Velocity

Fig.15 Comparison of Total Pressure Cp_{ol}, Static Pressure Cp_{sl} and Axial Velocity $\bar{u}_b$ Spanwise Distribution through the Wing Vortex Center at Section of $\bar{x}$=0.50 among Different Configurations

On the one hand, the delay of wing vortex bursting is one of the reasons why the aerodynamic characteristics can be improved at high angles of attack due to the presence of body strakes. On the other hand, there is another important reason to explain the improvement. That is, the body strakes make the wing vortex intensity increase.

In the present experiments, there are two facts to indicate the body strakes increasing the wing vortex intensity. First of all, the tangential velocities at the points with identical distance from the vortex center are listed in Table 4. It is found that for configurations with body strakes the tangential velocity increases obviously, if compared with the Basic Configuration. It is easy to understand that an increase of tangential velocity means an increase of vortex intensity. Comparing the effect of body strake on increasing vortex intensity, it is found that the body strake $1^{\#}$ is more efficient than $2^{\#}$. Secondly, the decrease of static pressure in the vortex core due to the presence of body strakes (Fig.15(b)) also indicates that the wing vortex intensity increase. The decrease of static pressure in the wing vortex core certainly result in the increase of vortex lift acting on the wing.

V. Results of Flow Visualization

Fig.16 shows the comparison of the wing leading-edge vortex bursting positions between the Basic Configuration and Configuration $1^{\#}$ at different angles of attack. In the plot, C_r is a length of wing root chord. The left and right wing vortex bursting positions were recorded respectively because of the asymmetric and unsteady character of vortices at high angles of attack. The recorded data are roughly time-averaged values. Fig.16 indicates that the vortex bursting positions can be delayed if the configuration is mounted with body strakes.

Sectional flow patterns were visualized in order to observe the interferential phenomena of vortices and to understand vortex structural patterns. Fig.17 are a series of sectional vortex patterns for another configuration at α=24°. From these

Table 3. Comparison of Static Pressure Cp_{sl} at the Edge of Wing Vortex Core and Wing Vortex Stability between the Basic Configuration and Configuration $1^{\#}$ (α=24°)

Model	Test Section $\bar{x}$	Cp_{sl} (at the point with distance of 4mm from wing vortex center)	v_τ/v_b (at the point with distance of 3mm from wing vortex center)	φ (derived from v_τ/v_b)	k (derived from v_τ/v_b)
Basic Configuration	0.25	-4.27	0.79	38°	2.00
	0.45	-4.97	1.04	46°	1.28
	0.50	-4.80	1.24	51°	0.98
	0.55	-3.62	1.59	58°	0.68
Configuration $1^{\#}$	0.25	-3.39	0.51	27°	4.29
	0.50	-5.21	0.57	30°	3.50
	0.65	-3.90	0.79	38°	2.00
	0.70	-3.56	1.35	53°	0.87
	0.80	-1.30	1.47	56°	0.77

Table 4. Comparison of Tangential Velocity at the Point with 3mm Distance from the Wing Vortex Center (α=24°)

Model	Test Section $\bar{x}$	v_τ (at the left side of wing vortex center)	v_τ (at the right side of wing vortex center)
Basic Configuration	0.25	1.10	1.54
	0.45	0.66	0.80
	0.50	0.41	0.48
	0.55	0.07	0.57
Configuration 1#	0.25	1.24	2.10
	0.50	1.23	2.15
	0.65	0.45	1.23
	0.70	0.33	0.67
	0.80	0.13	0.43
Configuration 2#	0.25	1.02	1.65
	0.50	0.71	1.59

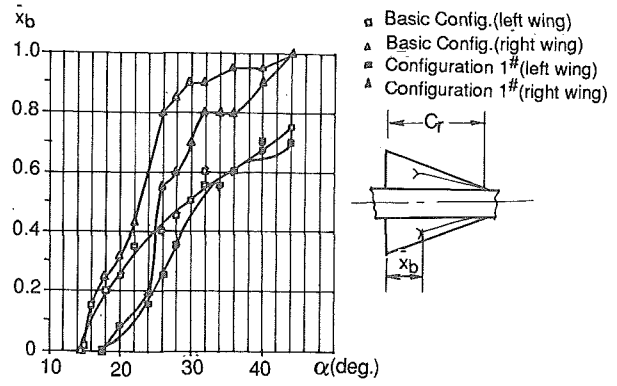

Fig.16 Comparison of Wing Leading-Edge Vortex Bursting Positions between the Basic Configuration and Configuration 1#

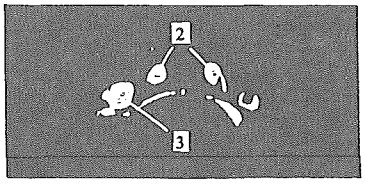

17(a) $\bar{x}$=0.0

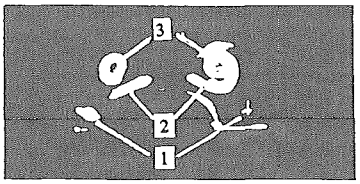

17(b) $\bar{x}$=0.2

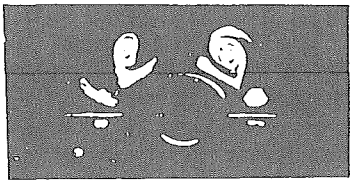

17(c) $\bar{x}$=0.3

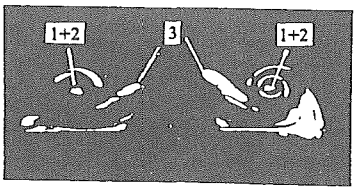

17(d) $\bar{x}$=0.5

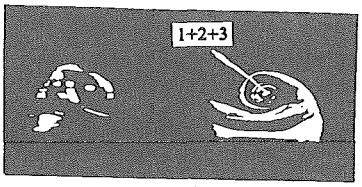

17(e) $\bar{x}$=0.6

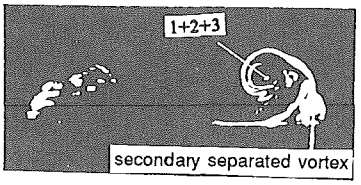

17(f) $\bar{x}$=0.7

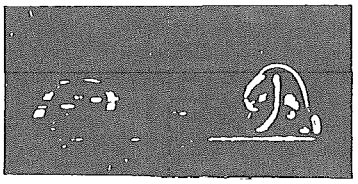

17(g) $\bar{x}$=0.7

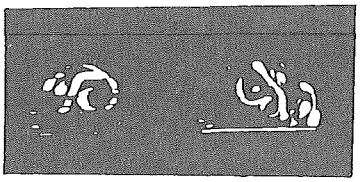

17(h) $\bar{x}$=0.8

1- wing vortex 2 - body vortex 3 - strake vortex

Fig.17 Cross-Sectional Vortex Flow Pattern of a Wing-Body Configuration

photographs, we can see the detail process of interferences among vortices, and there are some different interferential phenomena from those discussed above. It should be pointed out that the specific state of vortex flow field which results from vortex interferences, such as to induce, to move around and to merge each other among vortices, is quite different from each other. The specific state of vortex interferential flow field basically depends on the three factors, i.e., the vortex intensity, the vortex spatial track and the vortex distances from each other. While these factors further relate to the shape of the strake, the mounting position of the strake and the angle of attack of the configuration. So the vortex patterns shown in Fig.17 are the particular circumstances. Anyway, it is found that the different interferences finally all result in the delay of wing leading-edge vortex bursting.

VI. Conclusions

The main mechanism of favourable interferences of body strakes is as follows:

Because of the effect of body strake vortex, the wing leading-edge vortex bursting is delayed. This is an important factor to the improvement of aerodynamic characteristics at high angles of attack.

Experimental results show that the strake vortex makes the total pressure in the wing vortex core increase and static pressure decrease. This means the wing vortex gains an additional total energy and dynamic energy. The additional dynamic energy enable the wing vortex to overcome the adverse pressure gradient. And this is favourable to maintain the vortex flow. This point of view is also confirmed by the fact that the axial velocity profile of the wing vortex changes from the wake flow profile to jet flow profile due to the effect of body strake at the section of $\bar{x}$=0.50.

The calculation of measurement data indicates that the value of k, which is a parameter representing the stability factor of vortex flow, is increased and the spiral angle φ is decreased due to the presence of body strake. So the analyses by means of stability theory show that the effect of strake vortex can enhance the stability of wing vortex flow.

All these factors mentioned above are favourable to the delay of the wing vortex bursting.

Experimental results also show that the body strakes are capable of increasing the wing vortex intensity.

The delay of wing vortex bursting and the increase of wing vortex intensity both play important roles in the improvement of aerodynamic characteristics at high angles of attack.

References

1. Xia Xuejian, Feng Yanan, Liu Xiaofeng and Han Xiaotao: Influence of Body Cross-sectional Shape and Forebody Shape on the wing Leading- Edge Vortex Burst, *Chinese Aeronautical Science and Technology Documentation*, HJB890726, 1989.

2. Xia Xuejian, Feng Yanan and Wu Zuobing: Investigation of the Effect of Forebody Machines on Longitudinal Aerodynamic Characteristics of A Fighter Configuration at High Angles of Attack, *Chinese Aeronautical Science and Technology Documentation*, HJB900876,1990.

3. Liu Xiaofeng: An Experimental Investigation of the Effects of Body Strakes on the Aerodynamic Characteristics of Fighter at High Angles of Attack and Mechanism, *Master's Thesis, Beijing University of Aeronautics and Astronautics*, 1991.

4. Xia Xuejian, Feng Yanan, Liu Xiaofeng and Ma Shulin: Interference, Control and Utilization of Vortex on Fighter, *Chinese Aeronautical Science and Technology Documentation*, HJL910091,1991.

5. Qi Mengbu and Li Jingbo: Seven-Hole Probe for High Angle Flow Measurement in Subsonic Compressible Flow, Part I: Developing and Calibration of Probe, *Technical Report of Nan Jing Institute of Aeronautics*, 83-007(Aerodynamics),1983.

6. Everett, K. N., Gerner, A. A. and Durston, D. A.: Seven-Hole Cone Probes for High Angle Flow Measurement: Theory and Calibration, *J. of AIAA*, Vol.21, No.7, pp992-998,1983.

7. Leibovich, S.: The Structure of Vortex Breakdown, *Ann. Rev. Fluid Mech.*, Vol.10, pp221-246, 1978.

8. Earnshaw, P. B.: An Experimental Investigation of the Structure of a Leading-Edge Vortex, *A.R.C. R&M*, No.3281, 1962.

9. Bossel, H. H.: Stagnation Criterion for Vortex Flows, *J. of AIAA*, Vol.6, No.6, pp1192-1193, June, 1968.

10. Wedemeyer, E. H.: Stable and Unstable Vortex Separation, *AGARD CP-247*, No.13, 1978.